Proceedings of the 36th International Conference on Ocean, Offshore & Arctic Engineering
June 25-30, 2017, Trondheim, Norway

OMAE2017-61562

SLOSHING AND SWIRLING IN PARTIALLY LOADED PRISMATIC CHAMFERED TANKS

Gustavo M Karuka
Yokohama National University
Yokohama, Japan

Makoto Arai
Yokohama National University
Yokohama, Japan

Hideyuki Ando
Monohakobi Technology
Institute, Tokyo, Japan

ABSTRACT

In this study a sloshing experiment using a partially filled membrane tank model was carried out and compared with numerical simulation. The pressure was measured at 10 points and a load cell measured the longitudinal and transversal forces, under regular and irregular excitation. A 3D finite difference method based solver was used for the numerical simulation. When the prismatic tank length to breadth ratio is near 1, swirling, i.e., liquid free surface's rotating motion in the tank might occur when the tank is excited near its natural frequency, especially for medium and low tank filling levels. According to the experimental and simulation data, the magnitude of the forces and impact pressures in this situation can be significant and therefore cannot be neglected. Tank designs might use different length to breadth ratios (L_t/B_t) depending on the ship size and number of tanks, so the problem is worth being investigated. The L_t/B_t and the occurrence of swirling was then investigated. The pressure distribution when the swirling occurs is then compared with the 1st mode sloshing pressure distribution, and considerations about the tank safety are inferred

1 INTRODUCTION

For safety reasons LNG carriers are only allowed to operate under restricted filling levels. However, in the near future, partially filled tanks are highly required. This is for a number of reasons, such as the use of LNG as fuel, demand for flexibility in operation for LNGC, offshore LNG offload operations and so on.

Partial filling in membrane type tanks leads to sloshing, and the generated loads may endanger the tank's structural integrity. Therefore, it is fundamental to the ship designer to know the magnitude of the sloshing loads and under which conditions they occur.

After analyzing the ship and tank dimensions of a number of membrane-type LNG carriers, it was noted that the tanks in general have a similar cross-section shape, but vary in length according to the vessel size and the tank position in the ship. Tanks at the extreme aft and forward tend to be shorter in order to adjust to the hull's geometry.

Whenever the tank has a squared shaped free-surface, or in other words, length to breadth (L_t/B_t) ratio near one, not only sloshing, but swirling may also occur. Most sloshing studies focus on the sloshing loads, using tanks with L_t/B_t ratio far from 1. So although there are swirling studies for spherical shaped tanks for example in (Faltinsen & Timokha, 2013, Arai et al., 2016), it is hard to find information about the loads of swirling in membrane tanks.

In this paper, sloshing and swirling in a membrane-type LNG carrier tank is numerically simulated using a finite difference method developed by the authors (Arai, Cheng, Kumano & Miyamoto 2002) for partial and full load conditions.

2 NUMERICAL METHOD

The numerical method used in the analysis of sloshing was based on the finite difference technique. The numerical method is outlined below.

Governing Equations

A coordinate system o-xyz fixed to the moving tank was adopted. Assuming an incompressible and inviscid fluid, the equations governing the liquid cargo motion inside the tank are the mass continuity equation

$$\frac{\partial u}{\partial x}+\frac{\partial v}{\partial y}+\frac{\partial w}{\partial z}=0 \qquad [1]$$

and Euler's equations of motion:

$$\begin{aligned}
&\frac{\partial u}{\partial t}+u\frac{\partial u}{\partial x}+v\frac{\partial u}{\partial y}+w\frac{\partial u}{\partial z}=-\frac{\partial P}{\rho\partial x}+\frac{f_x}{\rho}\\
&\frac{\partial u}{\partial t}+u\frac{\partial v}{\partial x}+v\frac{\partial v}{\partial y}+w\frac{\partial v}{\partial z}=-\frac{\partial P}{\rho\partial y}+\frac{f_y}{\rho} \qquad [2]\\
&\frac{\partial u}{\partial t}+u\frac{\partial w}{\partial x}+v\frac{\partial w}{\partial y}+w\frac{\partial w}{\partial z}=-\frac{\partial P}{\rho\partial z}+\frac{f_z}{\rho}.
\end{aligned}$$

Where

u, v, w: velocity components with respect to the coordinates fixed to the tank;

f_x, f_y and f_z: x, y and z components of external forces,

p: pressure,

ρ: density of the liquid.

The exciting motion of the tank is taken into account by the external forces f_x, f_y and f_z in the motion equations.

Finite Difference Approximation

To reduce the computational time and to simplify the numerical method, a staggered mesh system with constant grid spacing Δx, Δy and Δ z in the x, y and z directions was used. The variables u, v and w were evaluated at the cell faces, while p was evaluated at the center of the grid cells. Once the initial conditions of the problem were applied, the velocities u, v and w were estimated for the next time step by using the motion equations. The variables u, v, w and p were iteratively adjusted to satisfy the continuity equation and boundary conditions. Details can be found in (Arai et al., 2002, Cheng and Arai, 2003 and 2005).

Rigid wall

Rigid boundaries are modeled by setting zero normal velocity on the wall. Free-slip with the assumption of inviscid was used.

Free Surface

The position of the free surface was evaluated by using a height function H, whose value was updated at every time step by applying the kinematic condition:

$$\frac{\partial h}{\partial t}+u\frac{\partial h}{\partial x}+v\frac{\partial h}{\partial y}=w \qquad [3]$$

where H=H(t,x,y) is the height of the free surface measured from the tank bottom and is a function of t, x and y. The atmospheric pressure p_{atm} is set at the free surface location.

Impact on tank ceiling

To achieve a stable assessment of the impact pressure at the tank ceiling, a transition of the boundary condition from a free surface to a rigid wall proposed by Arai, Cheng, Kumano & Miyamoto (2002) and Cheng & Arai (2003) is considered. A detailed explanation of this condition can also be found in Cheng & Arai (2005).

3 EXPERIMENT SETUP

A series of model experiment were carried out at Monohakobi Technology Institute (MTI) Yokohama Laboratory, as shown in Figure 1. A 1:40 scale tank was used with mounting on a moving table (Figure 1, left). Ten pressure gauges of Kyowa PS-05KD were placed along the walls. The table was excited with a regular sway motion. A smaller model tank of 1:68.75 scale was also used to measure transverse and longitudinal forces acting on the tank (Figure 1, right) by using a two directional load cell. The configurations of the two tanks are exactly the same and only the tank size were different.

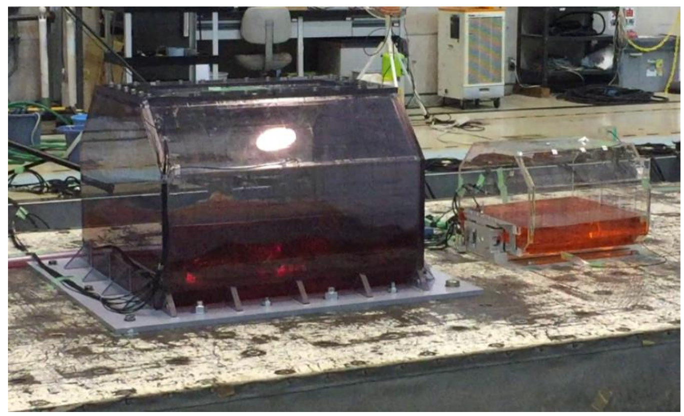

Figure 1 - picture of tanks and moving table

Tank geometry and pressure gauge location

The model tank is a scale of a membrane tank with the Length x Breadth x Depth dimensions of 971x 952 x 689 mm. The internal geometry of the tank and the position of the pressure gauges can be seen in Figure 2.

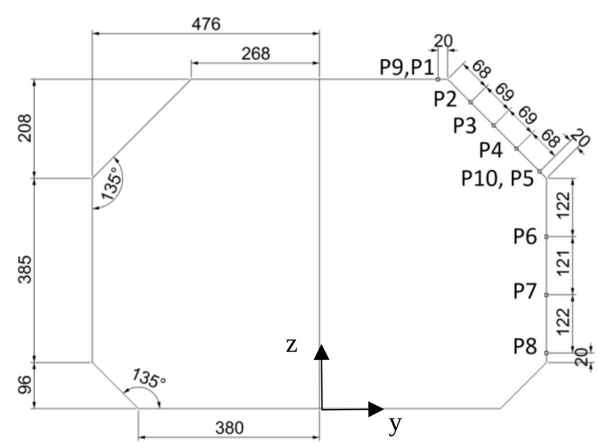

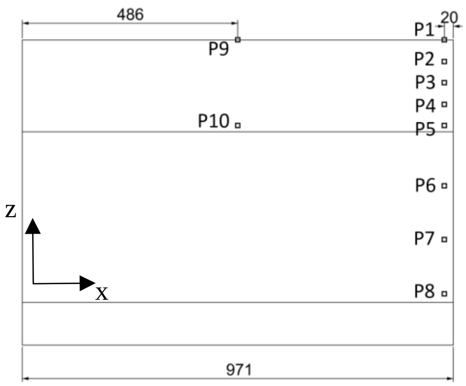

Figure 2 – dimensions of tank model (units in mm)

Experiment cases

In Table 1, the parameters used in the model test are presented. The table was excited near the natural frequency for each filling level. Then natural frequency f_N was estimated by an simple linear theory suggested by (Abrahamson, 1974) for rectangular shaped tanks in eq. [4]. A small adaptation was applied however. Instead of using the tank fixed breadth B_t in the equation, the free-surface breadth given a certain filling level was used when the free-surface was located at the tank chamfers.

$$f_N = \frac{\sqrt{(g\pi / B_t)\tanh(\pi h / B_t)}}{2\pi} \qquad [4]$$

Table 1 – test cases

Type	regular sway
Amplitude	20 mm
Frequency	f_1, f_1+0.02,f_1-0.02 Hz
Filling level	30%, 50%, 70%, 80%, 90%, 95%
Direction	90deg.

4 RESULTS

Comparison with experimental data

The numerical simulations were run with the same conditions as the experiment. The mesh divisions used were 34x34x29. The pressures were measured at the cell corresponding to the pressure gauge locations. It is important to note that all the pressure data shown on this study is the dynamic pressure, which discounts the effect of the hydrostatic pressure corresponding to the height of the initial free-surface. The dynamic pressure was made non-dimensional by using the tank height h_t.

As shown in Figure 3, it is possible to see the change in the pressure located in P8 with time, where sloshing developed gradually until it reaches a transition zone between sloshing and swirling. A fully developed swirling occurs after around $t = \sqrt{B_t/g}$=80. According to Figure 3, the computational and the experimental results overlap and appear as one. Therefore, the time scale was enlarged and shown in Figure 4 and Figure 5. It can be observed that sloshing has 2 peaks while swirling has only one peak.

Figure 6 and Figure 7 shows the same conditions but for the pressure gauge P5, located at the lower part of top chamfer. The pressure magnitude for swirling in this case decreases in comparison with sloshing. The impact pressure measured at P5 has a larger scatter in the experiment than numerical computation. Occasional impact pressure also occurs in swirling in the experiment.

Swirling can be clearly seen for 30% and 50% filling conditions. For 70%, 80%, 90% and 95% the phenomena was small or negligible. The reason is that the top chamfer is located near the 70% height. Above this height, the horizontal section of the tank is no longer a square.

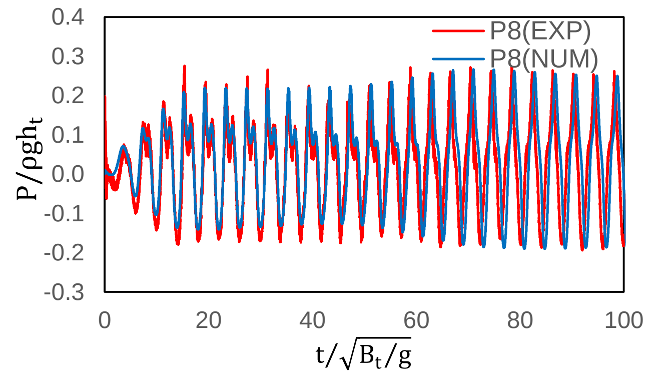

Figure 3 - 50%filling level, sloshing, $f/\sqrt{g/B_t} = 0.250$, P8

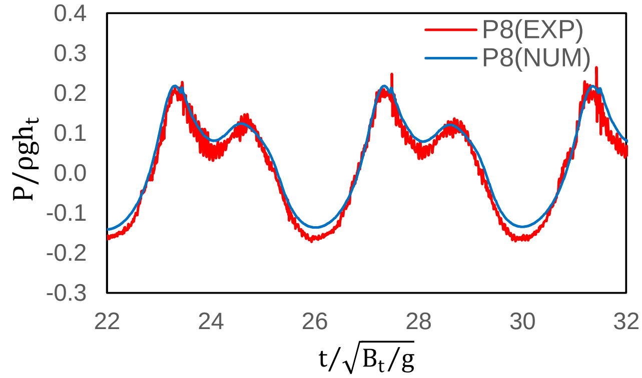

Figure 4 - 50%filling level, sloshing, $f/\sqrt{g/B_t} = 0.250$, P8

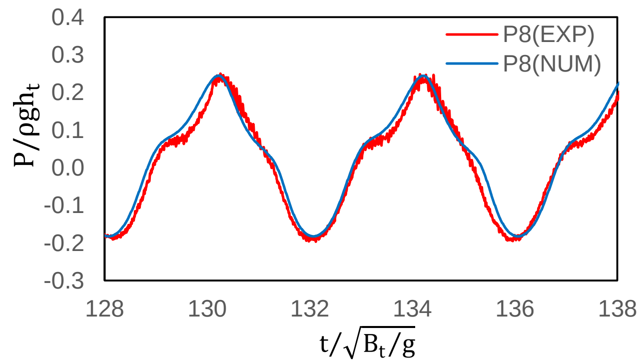

Figure 5- 50%filling level, swirling, $f/\sqrt{g/B_t} = 0.250$, P8

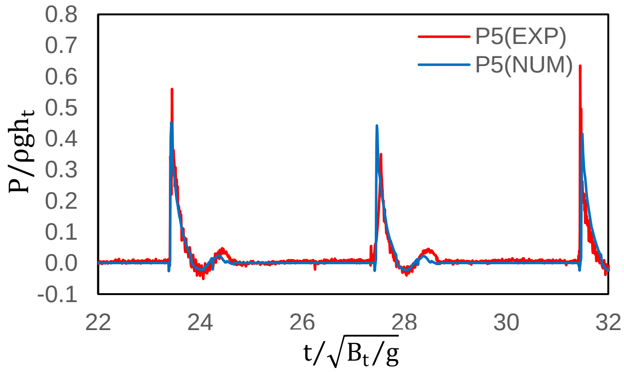

Figure 6- 50%filling level, sloshing, $f/\sqrt{g/B_t} = 0.250$, P5

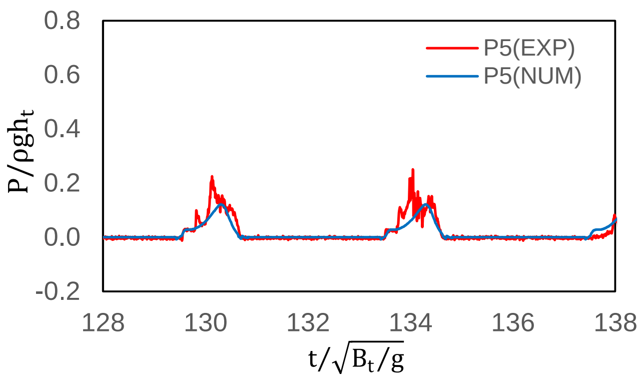

Figure 7 - 50%filling level, swirling, $f/\sqrt{g/B_t} = 0.250$, P5

A 90% filling level conditions was also tested. Figure 8 and Figure 9 show the measured pressures at P1 and P5. Both of them show good agreement with numerical computations in general, but there was a tendency that in the experiments, occasionally the impact pressure had higher peaks in comparison with the simulation. This is not a surprise, since very local effects such as a very small deformation of the free surface cannot be captured by a numerical simulation.

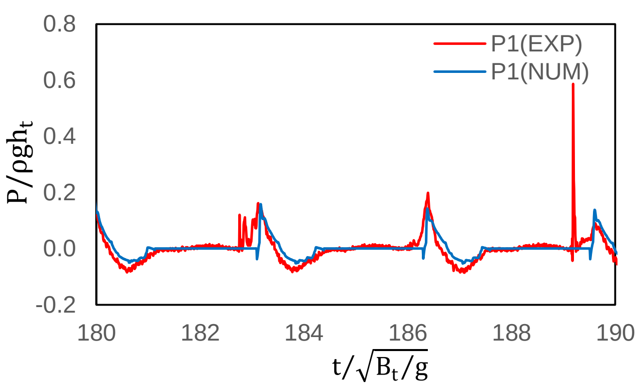

Figure 8 - 90%filling level, $f/\sqrt{g/B_t} = 0.312$, P1

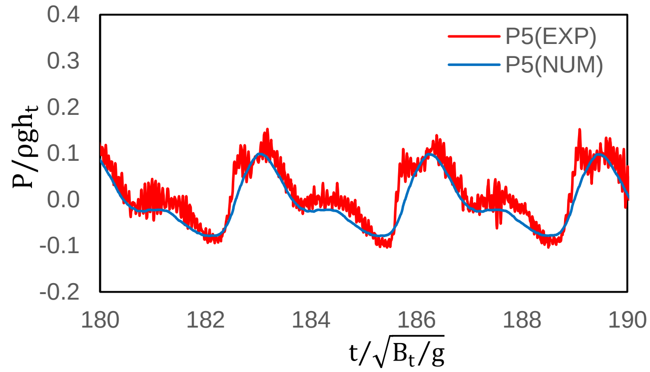

Figure 9 - 90%filling level, $f/\sqrt{g/B_t} = 0.312$, P5

Considerations about swirling

When sloshing occurs, two peaks appear at the bottom pressure of the tank as shown in Figure 10: the first peak is generated when the liquid surface reaches its maximum height, so the hydrostatic pressure at the bottom is high. The second peak occurs when the liquid is going down and the dynamic pressure increases. This relation can be understood from the free surface motion shown in Figure 11.

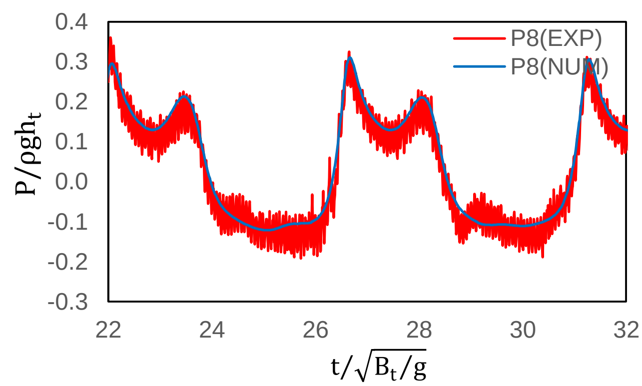

Figure 10 - 30%filling level, sloshing, $f/\sqrt{g/B_t} = 0.215$, P8

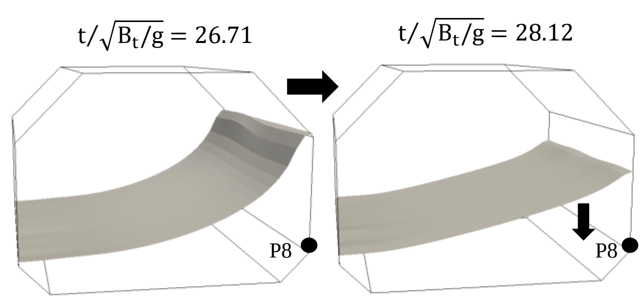

Figure 11 – snapshots of free surface on sloshing

In the swirling case, on the other hand, the liquid surface sometimes raises twice in one cycle, resulting in four peaks, as in Figure 12 and Figure 13. As show in Figure 13, the liquid reaches a maximum height in snapshots 1 and 3, and go downwards in snapshots 2 and 4. Snapshots 1 and 4 have almost the same shape, with the difference that the elevate wave happens in the front and aft of the tank, respectively.

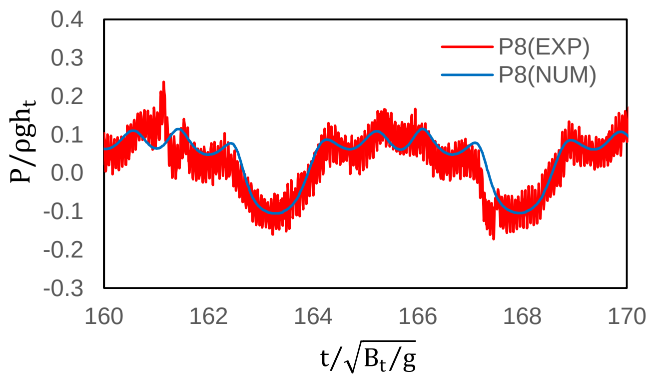

Figure 12 - 30%filling level, swirling, $f/\sqrt{g/B_t} = 0.215$, P8

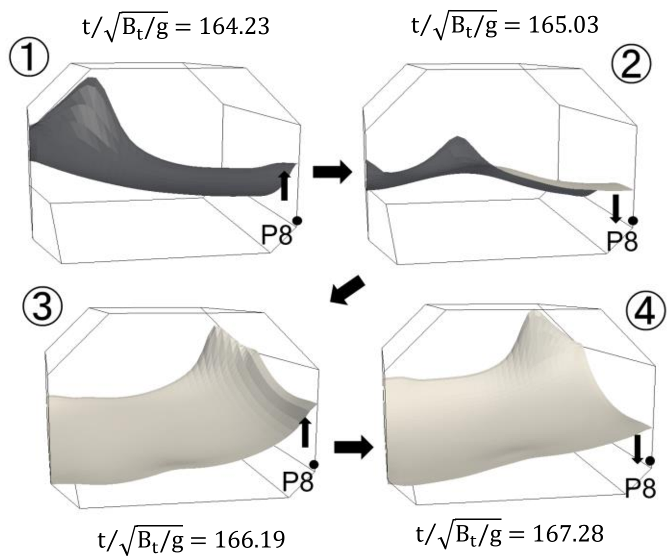

Figure 13 - snapshots of free surface on swirling

Influence of initial condition

As for the rotation direction for swirling both clockwise and counter-clockwise direction appeared in the model experiment. The rotation direction seems to be sensitive to small disturbances, such as initial free-surface geometry and model tank imperfections.

In the numerical computation, because the excitation is two-dimensional, the response is also two-dimensional, in other words, pure transversal sloshing. However very small numerical errors trigger the excitation in the longitudinal direction and eventually swirling occurs.

It is easy to identify the occurrence of swirling by observing the increase of the longitudinal force F_x on the tank caused by the liquid. When the swirling is fully developed, the magnitude of the transverse force F_y and longitudinal force F_x become nearly equal, which are shown in Figure 14(a).

By introducing a small inclination (about 1 degree) intentionally to the free-surface at the initial condition, the swirling occurs earlier as shown in Figure 14 (b).

It is interesting to note that in general, the transversal forces caused by sloshing are bigger than the transversal forces caused by swirling.

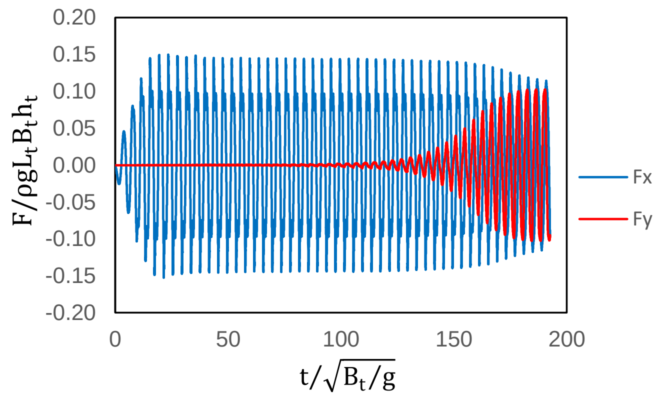

(a) Initial free surface inclination: 0 degree

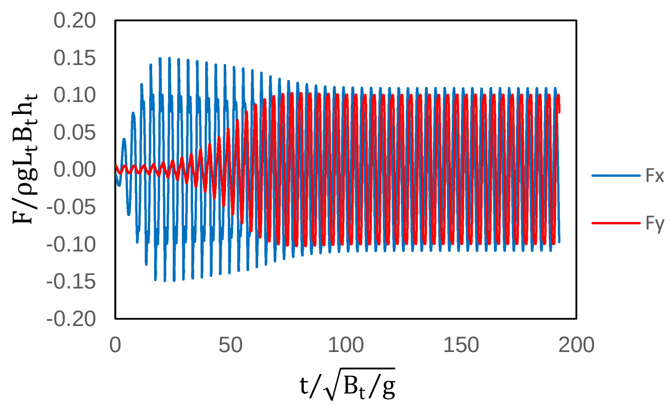

(b) Initial free surface inclination: 1 degree

Figure 14 – computed transversal and longitudinal forces (50%filling level, $f/\sqrt{g/B_t} = 0.250$, (sway amplitude)/B_t = 0.021)

Pressure distribution in the tank

In this section, the results of the simulations carried out for 60 cycles are shown. Figure 15 shows the total pressure distribution (a) and the dynamic pressure (b).

The dynamic pressure was calculated by subtracting the static pressure from the total pressure. The static pressure was calculated based on the initial liquid height.

As shown in Figure 15, in the 50% filling level condition, the critical point for slosh impact pressure is near the lower part of the top chamfer. For the swirling case, in Figure 16, the pressure in the chamfer is not elevated as in the sloshing, but a high pressure occurs at the top chamfer corner when there is contact with the crest of the free-surface. The magnitude of the impact was similar to the sloshing in this case, which suggests that the impact pressure caused by swirling may not be negligible.

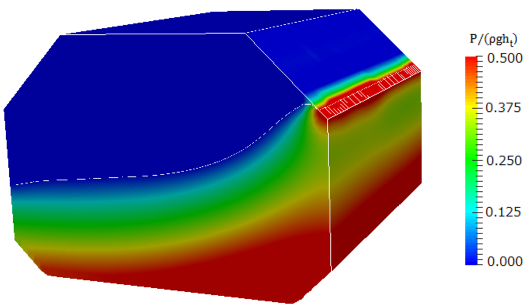

(a) Total pressure

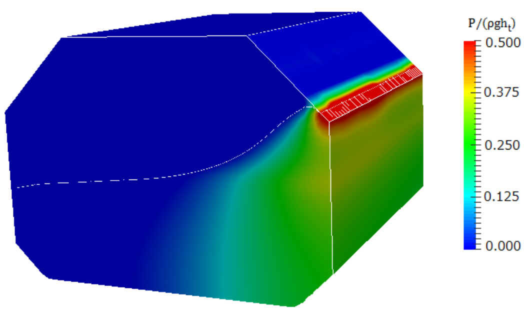

(b) Dynamic pressure

Figure 15 - snapshot of pressure for sloshing (50%filling level, $f/\sqrt{g/B_t} = 0.250$, (sway amplitude)/B_t = 0.021)

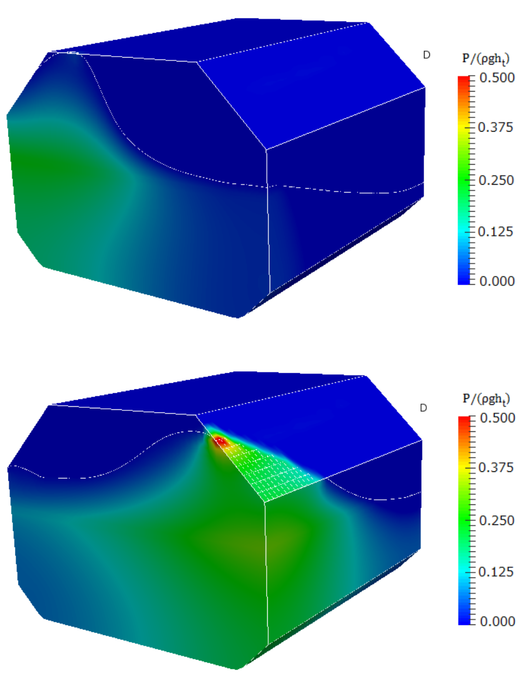

Figure 16 - snapshot of dynamic pressure for swirling (50%filling level, $f/\sqrt{g/B_t} = 0.250$, (sway amplitude)/B_t = 0.021)

Figure 17, Figure 18, Figure 19 and Figure 20 show the maximum dynamic pressure distribution for the whole simulation time for 30%, 50%, 90% and 95% filling levels. For 30% and 50% it can be observed that the lower part of the top chamfer suffers the highest pressure. Note that for 50%, in the maximum pressure distribution there is a slight increase in pressure at the top chamfer corner due to swirling. For 90% filling level, not a significant dynamic pressure is detected. For 95%, high pressure appears at the ceiling edge, especially near corners. This suggests that tanks with filling levels near the full load condition may also be susceptible to high impact pressure.

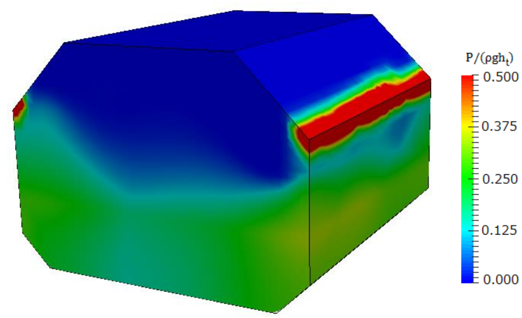

Figure 17 – max dynamic pressure (30%filling level, $f/\sqrt{g/B_t} = 0.215$, (sway amplitude)/B_t = 0.021)

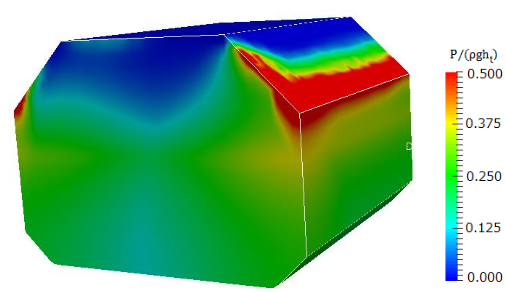

Figure 18 – max dynamic pressure (50%filling level, $f/\sqrt{g/B_t} = 0.250$, (sway amplitude)/B_t = 0.021)

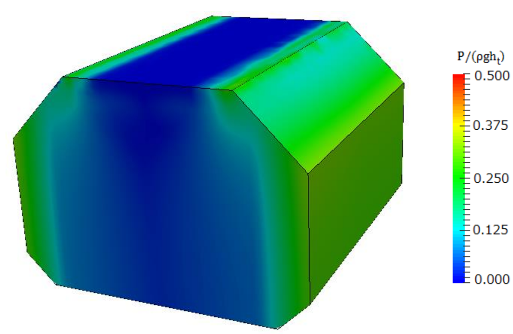

Figure 19 - max dynamic pressure (90%filling level, $f/\sqrt{g/B_t} = 0.312$, (sway amplitude)/B_t = 0.021)

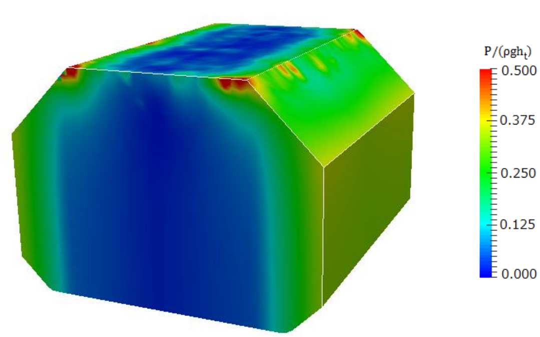

Figure 20 - max dynamic pressure (95%filling level, $f/\sqrt{g/B_t} = 0.333$, (sway amplitude)/B_t = 0.021)

Swirling for different L_t/B_t ratios

In Figure 14 it is possible to see the relation between transverse and longitudinal forces. When the square shaped tank is excited in sway, swirling develops and F_x and F_y tend to have the same magnitude. In Figure 14 case, when swirling is fully developed the ratio of F_x/F_y is about 0.92.

In order to understand the swirling for tanks with different L_t/B_t ratio, the tank model used in the study was slightly modified and tested. The tanks were excited with a regular sway excitation (Amplitude/B_t) of 0.021. Basically the L_t dimension was changed keeping the other parameters the same as Figure 2. Figure 21 and Figure 22 show the F_x/F_y ratio for tanks with different L_t/B_t ratio for two conditions: 50% and 30% filling levels. It can be clearly seen that the swirling occurs with high intensity when L_t/B_t ratio is near 1. For both cases swirling still occurs, although in different intensities, in a range that goes approximately from L_t/B_t of 0.9 to 1.10.

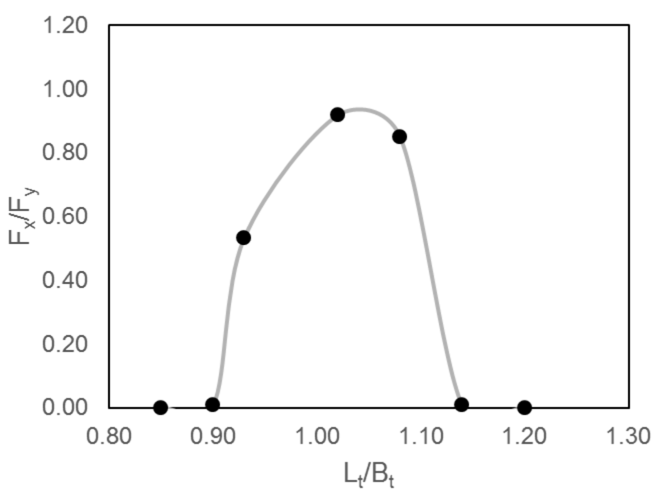

Figure 21 –relation of swirling and length to breadth ratio for 50% filling level , $f/\sqrt{g/B_t} = 0.250$

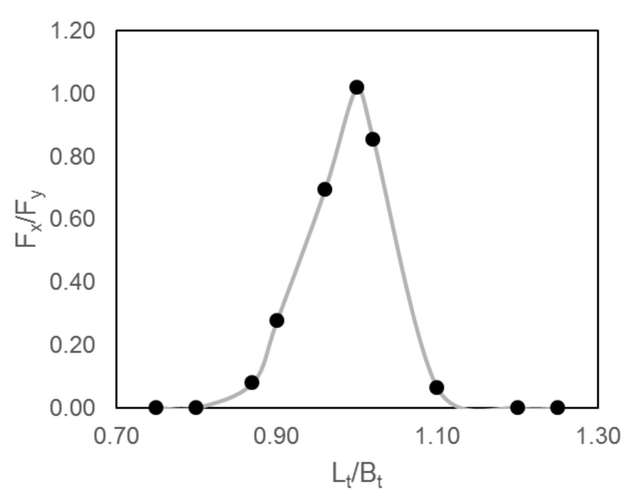

Figure 22 –relation of swirling and length to breadth ratio for 30% filling level, $f/\sqrt{g/B_t} = 0.215$

5 CONCLUSIONS

In this study a series of simulations for different filling levels were carried out and compared with experimental data. The general fluid motion and dynamic pressures obtained by our numerical simulation agreed very well with experimental data, which confirms the suitability of the numerical tool to represent the phenomenon. However very localized impact pressures are sometimes not well captured in the simulation. This may be mainly due to the small deformations of the free surface caused by local disturbances such as droplet of the water generated by the free surface impacts on the tank wall, etc.

For middle to low filling levels, swirling can occur if the length to breadth ratio of the tank is near 1. Swirling can be important for some tank geometries and although the non- impulsive pressures were lower in comparison with sloshing, the localized impulsive pressure can be significant and it may have almost the same magnitude of that of the sloshing.

A 3D representation of the maximum dynamic pressure were shown. It is possible to see that although high filling levels are accepted as safe filling levels, considerably high impact pressure can still occur at the tank ceiling, and this should be noted by the designers.

Future tasks

In this paper a tank with L_t/B_t ratio near 1 was studied. It is necessary to examine further the swirling loads for different L_t/B_t ratio. It was concluded that when swirling occurs, the impact pressure caused by the fluid motion is not negligible. However, it is necessary to confirm in further the studies how often swirling occurs in practical operations. In this case the occurrence of swirling in irregular seaways must be analyzed.

6 ACKNOWLEDGMENTS

Part of this research was carried out as ClassNK's Joint R&D with Industries and Academic Partners project. The authors would like to express their gratitude to ClassNK and Monohakobi Technology Institute (MTI) for their financial support.

7 REFERENCES

Abramson, H. M., Bass R. L., Faltinsen, O, Olsen, HA. (1974), Liquid Slosh in LNG Carriers, 10th Naval Hydro-Dynamics Symposium, pp.21-38.

Arai, M., Cheng, L. Y., Kumano, A., Miyamoto, T., A. (2002) "Technique for Stable Numerical Computation of Hydrodynamic Impact Pressure in Sloshing Simulation," Journal of the Society of Naval Architects, Japan, Vol. 191, pp. 299-307.

Arai M., Cheng L.Y., Wang X., Okamoto N., Hata R., Gustavo M.K.(2016) . "Sloshing and swirling behavior of liquid in a spherical LNG tank", Proceedings of International Symposium on Ships and Other Floating

Structures PRADS 2016.

Cheng, L. Y., Arai, M. (2003). "A Technique for Stable Numerical Assessment of Hydrodynamic Impact Pressure Due to Sloshing in Chamfered Tanks", Conference Proceedings, The Society of Naval Architects of Japan, Vol. 1, pp. 105-106.

Cheng, L. Y., Arai, M. (2005) “A 3D Numerical Method for Assessment of Impact Loads Due to Sloshing in Liquid Cargo Tanks,” Proceedings of the Fifteenth International Offshore and Polar Engineering Conference, pp. 214-221.

Faltisen, O.M., Timokha A. (2013). “Nonlinear sloshing in a spherical tank”, Conference Proceedings, OMAE.

